A Novel Approach for Monitoring Zonal Irregularity Drift using a Stand-Alone GNSS Scintillation Monitor

Charles S. Carrano, Keith M. Groves, Susan H. Delay, and Patricia H. Doherty
Institute for Scientific Research, Boston College, Boston, MA

BIOGRAPHY

Charles S. Carrano is a senior research physicist and Principal Investigator at Boston College's Institute for Scientific Research. He has authored and co-authored more than 40 technical papers concerning the impacts of ionospheric scintillation on radar, satellite communications, and Global Navigation Satellite Systems (GNSS). He is an Associate Editor of the AGU journal Radio Science, and serves on the Editorial Board of GPS Solutions. He has a B.S. degree from Cornell University and M.S. and Ph.D. degrees from The Pennsylvania State University.

Keith Groves works as a Senior Research Scientist at Boston College where his research interests include radio wave scintillations, high power HF ionospheric modification, wave-particle interactions, and space weather impacts on communication, navigation and surveillance systems. He has authored and co-authored more than 60 papers and is an internationally recognized expert in the field of ionospheric scintillations. He has a Ph.D. in Space Physics from MIT and a B.S. in Physics from Andrews University.

Susan Delay is a Senior Research Analyst with the Boston College ISR. Her work includes data and numerical analysis, programming and graphics development.

Patricia Doherty is Director of the Institute for Scientific Research at Boston College. She has been an active researcher in the area of radio wave propagation for the past 20 years, focusing on ionospheric effects on satellite-based navigation. She has led ionospheric research in support of Satellite-Based Augmentation Systems (SBAS), of which the FAA's Wide Area Augmentation System (WAAS) is an example. She has served in numerous volunteer offices in the Institute including the ION's Executive Committee and as program and general chair of the ION GNSS meeting. She is currently executive vice president of the Institute.

ABSTRACT

A complete characterization of field-aligned ionospheric irregularities responsible for the scintillation of GNSS satellite signals includes not only their spectral properties (power spectral strength, spectral index, outer-scale, and anisotropy) but also their bulk motion, or drift. At low latitudes, the irregularity drift is predominantly zonal and controlled by the F region dynamo and regional electrodynamics. These physical processes are of considerable interest and are currently investigated using a variety of measurement techniques. From a system impacts perspective, the irregularity drift is important because it affects the rate of signal fading and the level of phase fluctuations encountered by the receiver (both of which influence its ability to maintain lock on the satellite signals).

The zonal irregularity drift is most commonly measured at low-latitudes by cross-correlating observations of a satellite signal made by a pair of closely-spaced receivers. The AFRL-SCINDA network operates a small number of VHF spaced-receiver systems at low latitude stations for this purpose. A far greater number of GNSS scintillation monitors are operated by AFRL-SCINDA (25-30) and the Low Latitude Ionospheric Sensor Network (35-50), but the individual receivers are too widely separated to monitor the drift using cross-correlation techniques. Previous authors have attempted to

measure the drift using a single GNSS receiver by cross-correlating the signals from different satellites, but differences in the satellite scan directions with respect to the field-aligned irregularities tend to degrade the correlation (thereby limiting the usefulness of this technique).

In this paper, we present an alternative approach that leverages the weak scatter scintillation theory [Rino, Radio Sci., 1979] to infer the zonal irregularity drift from single-station GNSS measurements of S_4, σ_φ, and the propagation geometry alone. Unlike the spaced-receiver technique, this approach requires assumptions regarding the height of the scattering layer (which introduces a bias in the drift estimates) and the spectral index of the irregularities (which affects the spread of the drift estimates about the mean). Nevertheless, theory and experiment show that the ratio of σ_φ to S_4 is less sensitive to these parameters than it is to the zonal drift. We validate the technique using VHF spacer-receiver measurements of zonal irregularity drift obtained from the AFRL-SCINDA network.

We believe this work may have important ramifications for the high-latitude ionospheric community, who commonly observe phase without amplitude scintillations at high latitudes and therefore tend to study S_4 and σ_φ as if they were independent. Our results demonstrate that S_4 and σ_φ are closely related, with their ratio depending on the irregularity drift and propagation geometry more strongly than the structure of the irregularities or the geophysical processes by which they were created.

While the spaced receiver technique remains the preferred way to monitor the irregularity drift when closely pairs of receivers are available, our technique enables a new opportunity to monitor zonal irregularity drift using regional or global networks of widely separated GNSS scintillation monitors.

1. INTRODUCTION

Most methods for estimating the zonal irregularity drift in the equatorial ionosphere are variations of the spaced-receiver technique [Vacchione et al., 1987; Spatz et al., 1988]. In the spaced- receiver technique, the zonal irregularity drift is measured by cross-

correlating the power fluctuations (amplitude scintillation) observed from the same satellite signal using receivers separated by a known baseline distance. The technique has been applied extensively to signals from geostationary satellites and, more recently, also to GNSS satellite signals [de Paula et al. 2002; Ledvina et al, 2004].

When only a single GNSS receiver is available, or one located too distant from other receivers in a network, the spaced-receiver technique obviously cannot be employed in the traditional fashion. Nevertheless, earlier attempts have been made to measure the irregularity drift using a *stand-alone* GNSS receiver by correlating slant TEC observations between different satellites [Liang et al., 2009; Ji et al., 2011]. The difficultly with this approach is that the different scan directions of the satellites with respect to the field-aligned irregularities generally results in a low correlation coefficient, except in special cases. This precludes systematic estimation of the irregularity drift.

As an alternative to correlating slant TEC, Carrano et al. [2012a] proposed that the zonal irregularity drift may be measured using a stand-alone GNSS scintillation monitor by least squares fitting the spectrum of measured intensity fluctuations with a solution to the 4th moment equation governing fluctuations of the field. While effective, this approach is both complex to implement and computationally expensive. In this paper, we present a simpler approach that leverages the weak scatter scintillation theory [Rino et al., 1979] to infer the zonal drift from GNSS measurements of S_4 (RMS of intensity fluctuations), σ_φ (RMS of detrended carrier phase fluctuations), and the propagation geometry alone.

2. METHODOLOGY

The idea behind the technique we propose to measure the zonal irregularity drift is the following. According to the weak scatter theory (Rino, 1979) both S_4 and σ_φ depend on the irregularity strength and propagation geometry, but only σ_φ depends on the irregularity motion through the effective scan velocity (which is a measure of the speed and direction which the satellite ray-path scans through

the field-aligned irregularities). Essentially, S_4 is independent of the satellite and plasma motion while σ_φ is not. Our technique leverages this idea to infer the effective scan velocity from measurements of the ratio σ_φ / S_4. Once the effective scan velocity is known, the zonal irregularity drift may be calculated.

The model of ionospheric scintillation proposed by Rino [1979] is the most widely used and arguably the most successful. In this section we briefly review the model and establish the relationships it implies between the physical properties of the random ionospheric medium (notably the spectral index, anisotropy, and irregularity drift), the propagation geometry and satellite scan velocity, and the scintillation parameters that are readily measured with GNSS scintillation monitors, namely S_4, T, and σ_φ. S_4 and σ_φ are the intensity and phase scintillation indicies, and T is the phase spectral strength.

Rino assumed the following form for the spectral density function of the phase after one-way passage through a thin layer of field-aligned anisotropic ionospheric irregularities:

$$\Phi_\phi(\boldsymbol{\kappa}) = \frac{abC_p}{(\kappa_0^2 + A\kappa_x^2 + B\kappa_x\kappa_y + C\kappa_y^2)^{(p+1)/2}} \quad (1)$$

In the above p represents the phase spectral index. The turbulence is assumed to have outer scale L_0, and $\kappa_0 = 2\pi/L_0$ is the outer scale wavenumber. The parameters a and b are scaling factors that elongate contours of constant correlation along and transverse to the magnetic field, respectively. The ratio $a{:}b$ is the so-called axial ratio of rod-like field-aligned irregularities characteristics of plasma turbulence in the equatorial ionosphere. The transverse wavenumbers in the geomagnetic east and geomagnetic north directions are symbolized by κ_x and κ_y, respectively. The coefficients A, B, and C depend on the directions of propagation and the magnetic field, and are obtained by relating the propagation line of sight and the irregularity axes. Equations for A, B, and C are given in the Appendix. The parameter C_p is the strength of the 3-D spatial spectrum of phase evaluated at the wavenumber 1 rad m^{-1}:

$$C_p = r_e^2 \lambda^2 C_s L \sec\theta \quad (2)$$

In (2) r_e is the classical electron radius (2.8179x10^{-15} m), λ is the wavelength, C_s is the strength of the 3-D spatial spectrum of electron density fluctuations, L is the thickness of the scattering layer, and θ is the propagation (nadir) angle at the ionospheric penetration point (IPP).

Rino [1979] showed that for propagation through a thin layer of ionospheric irregularities in the Born approximation (single scatter), the S_4 index can be expressed as:

$$S_4^2 = C_p \rho_F^{p-1} F_S(p)\wp(p) \quad (3)$$

The Fresnel radius appearing in (3) is

$$\rho_F^2 = z \sec\theta / k, \quad (4)$$

z is the height of the scattering layer, and k is the free space signal wavenumber. The quantity $F_S(p)$ depends on p only and is given by

$$F_S(p) = \frac{\Gamma[(5-p)/4]}{2^{(p-1)/2}\sqrt{\pi}(p-1)\Gamma[(p+1)/4]} \quad (5)$$

The parameter $\wp(p)$ is a combined geometry and propagation factor which is given in equation 34 of Rino [1979]. Formulas needed to compute $\wp(p)$ are given in the appendix. We note the result (3) is valid when the scintillations are weak and the phase spectral index lies in the range $1 < p < 5$.

Consistent with the Rino power-law irregularity model and the Taylor assumption of frozen-in (non-evolving) flow, a 1-D time-series of phase fluctuations measured by a receiver on the ground is characterized by the one-dimensional temporal spectrum (from equations 16-18 in Rino, 1979)

$$\varphi(f) = \frac{T}{(f_0^2 + f^2)^{p/2}} \quad (6)$$

where f is the frequency and f_0 is the outer scale frequency. The 1-D phase spectral strength sampled at the frequency 1 Hz is

$$T = C_p F_T(p) G V_{eff}^{p-1} \quad (7)$$

In the above, G is the phase enhancement factor, which is given in the Appendix. The effective scan velocity, V_{eff}, relates the spatial sizes of structures encountered along the satellite scan to the temporal frequencies at which they appear in the measured 1-D time series of phase. For example, the frequency at which the outer scale is detected in the spectrum of measured phase fluctuations is $f_0 = V_{eff}/L_0$. The quantity $F_T(p)$ depends only on the spectral index and is equal to

$$F_T(p) = \frac{\sqrt{\pi}\,\Gamma[p/2]}{(2\pi)^{p+1}\Gamma[(p+1)/2]} \qquad (8)$$

Ratio of Phase to Amplitude Scintillation

Dividing (7) by (3) gives the important ratio

$$\frac{T}{S_4^2} = \left[\frac{F_T(p)}{F_S(p)}\right]\left[\frac{G}{\wp(p)}\right]\left[\frac{V_{eff}}{\rho_F}\right]^{p-1} \qquad (9)$$

Note that in equation (9) no measure of the irregularity strength remains, since C_p cancels in the division. The first factor in brackets is a function of the phase spectral index p only. The second factor in brackets depends on p and also the details of the propagation and satellite scan geometries. Knowledge of these, together with measurement of S_4 and T allows one to infer the effective scan velocity:

$$V_{eff} = \rho_F\left[\frac{F_S(p)}{F_T(p)}\frac{\wp(p)}{G}\frac{T}{S_4^2}\right]^{\frac{1}{p-1}} \qquad (10)$$

Some GNSS scintillation monitors do not measure the phase spectral strength T, and instead characterize phase scintillations in terms of the phase scintillation index σ_φ, which is the standard deviation of detrended phase scintillations. Assuming the time constant of the high pass filter used to detrend the phase measurements satisfies $\tau_c \ll L_0/V_{eff}$, the phase spectrum is well approximated by an unmodified power law over the range of interest (i.e. the outer scale can be ignored). In this case the defining relationship

$$\sigma_\varphi^2 = \int_{-\infty}^{\infty}\frac{T}{(f_0^2 + f^2)^{p/2}}df$$

$$\approx 2T\int_{\tau_c^{-1}}^{\infty} f^{-p}\,df \qquad (11)$$

can be integrated to give:

$$\sigma_\varphi^2 = \frac{2T}{p-1}\tau_c^{p-1} \qquad (12)$$

which can be written

$$\sigma_\varphi^2 = \frac{2}{p-1}C_p F_T(p)G\left[\tau_c V_{eff}\right]^{p-1} \qquad (13)$$

While it is possible to include the outer scale in the calculation above, this is generally not necessary for equatorial irregularities when the traditional choice of $\tau_c = 10$sec is made. Using (9) and (12) the ratio of S_4 and σ_φ can be expressed:

$$\frac{\sigma_\varphi^2}{S_4^2} = \left[\frac{2}{p-1}\frac{F_T(p)}{F_S(p)}\right]\left[\frac{G}{\wp(p)}\right]\left[\frac{\tau_c V_{eff}}{\rho_F}\right]^{p-1} \qquad (14)$$

This can be solved for the effective scan velocity to give

$$V_{eff} = \frac{\rho_F}{\tau_c}\left[\frac{p-1}{2}\frac{F_S(p)}{F_T(p)}\frac{\wp(p)}{G}\frac{\sigma_\varphi^2}{S_4^2}\right]^{\frac{1}{p-1}} \qquad (15)$$

Comparing the two formulations (9) and (15) for measuring the effective drift velocity, the former is more direct since it does not depend on the phase detrending filter cutoff.

Estimating the Zonal Irregularity Drift

The effective scan velocity is given in Rino's paper [1979] as his equation (13), repeated below:

$$V_{eff}^2 = \frac{CV_{sx}^2 - BV_{sx}V_{sy} + AV_{sy}^2}{AC - B^2/4} \qquad (16)$$

In the above, V_{sx}, V_{sy} are the magnetic northward and eastward components of the plasma velocity relative

to the scan velocity of the raypath at the ionospheric penetration point. Neglecting possible northward and vertical components of the irregularity drift (i.e. we assume that the irregularity drift is purely zonal), we can write:

$$V_{sx} = -V_{sx0}$$
$$V_{sy} = V_D - V_{sy0} \qquad (17)$$

where

$$V_{sx0} = V_{px} - \tan(\theta)\cos(\varphi)V_{pz}$$
$$V_{sy0} = V_{py} - \tan(\theta)\sin(\varphi)V_{pz} \qquad (18)$$

and V_{px}, V_{py}, and V_{pz} are the magnetic northward, magnetic eastward, and downward components of the ray-path velocity at the IPP. The terms involving $\tan(\theta)$ in (18) account for the horizontal translation of the continuously displaced coordinate system employed by Rino's model as it follows the propagation ray path.

Once the effective scan velocity has been computed from measurements of S_4 and T, or measurements of S_4 and σ_φ, we can compute the zonal irregularity drift velocity, V_D by solving the quadratic equation for it implied by (16) -(18), whose solution is

$$V_D = V_{D0} \pm \frac{1}{A}\sqrt{(AC - B^2/4)(AV_{eff}^2 - V_{sx0}^2)} \quad (19)$$

where

$$V_{D0} \equiv V_{sy0} - \frac{B}{2A}V_{sx0} \qquad (20)$$

The velocity V_{D0} is generally on the order of 40 m/s for GPS satellite orbits in the equatorial zone where the irregularities are highly elongated. It is a purely geometrical factor which does not depend on the irregularity velocity. Thus, when the irregularities are drifting eastward at speeds exceeding 40 m/s (which is typical) the positive root should be chosen in (19) to obtain the zonal irregularity drift.

Model Simplifications for Equatorial Irregularities (the Infinite Axial Ratio Assumption)

As noted by Rino [1979], "In a highly anisotropic medium ($a \gg 1$ and $b = 1$) with propagation angles well removed from the direction of the principal axis" the propagation and geometry parameter $\wp(p)$ simplifies to

$$\wp(p) \sim \frac{\Gamma[p/2]}{\sqrt{\pi}\Gamma[(p+1)/2]} \qquad (21)$$

In fact, this approximation is a poor one unless the propagation is very nearly perpendicular to the magnetic field. A much better approximation, which is valid when $a \gg 1$ and $b = 1$ for any propagation direction and magnetic field orientation, is the following:

$$\frac{\wp(p)}{G} \sim \frac{\Gamma[p/2]}{\sqrt{\pi}\Gamma[(p+1)/2]} \qquad (22)$$

This approximation is accurate to within 0.1% for highly elongated irregularities with a 50:1 axial ratio (this axial ratio is assumed by the Wideband Scintillation Model, WBMOD [Secan et al., 1995]), at least for the propagation and scan geometries we encountered. With this approximation the two relatively complicated geometrical parameters G and $\wp(p)$, appearing in (10) and (15), cancel. These equations then reduce to

$$V_{eff} = \rho_F Q_T(p)\left[\frac{T}{S_4^2}\right]^{\frac{1}{p-1}} \qquad (23)$$

and

$$V_{eff} = \frac{\rho_F}{\tau_c}Q_\sigma(p)\left[\frac{\sigma_\varphi}{S_4}\right]^{\frac{2}{p-1}} \qquad (24)$$

The expressions (23) and (24) may be considered principal results of this paper. The factors $Q_T(p)$ and $Q_\sigma(p)$ appearing in the above are given by

$$Q_T(p) \approx \left[\frac{F_S(p)}{F_T(p)} \frac{\Gamma[p/2]}{\sqrt{\pi}\,\Gamma[(p+1)/2]} \right]^{\frac{1}{p-1}}$$

$$= \left[\frac{2^{(p+3)/2}\pi^{p-1/2}\Gamma[(5-p)/4]}{(p-1)\Gamma[(1+p)/4]} \right]^{\frac{1}{p-1}} \quad (25)$$

and

$$Q_\sigma(p) \approx \left[\frac{p-1}{2} \frac{F_S(p)}{F_T(p)} \frac{\Gamma[p/2]}{\sqrt{\pi}\,\Gamma[(p+1)/2]} \right]^{\frac{1}{p-1}}$$

$$= \left[\frac{2^{(p+1)/2}\pi^{p-1/2}\Gamma[(5-p)/4]}{\Gamma[(1+p)/4]} \right]^{\frac{1}{p-1}} \quad (26)$$

When $a \gg 1$ and $b = 1$ the exact form given in (16)-(18) for the effective scan velocity simplifies as well:

$$V_{eff}^2 \approx \frac{1}{QF}[(V_{px}\sin\psi - V_{pz}\cos\psi)\sin\varphi\tan\theta$$
$$+ (V_{py} - V_D)(\cos\psi - \cos\varphi\sin\psi\tan\theta)]^2 \quad (27)$$

where

$$QF^2 = \sin^2\varphi\tan^2\theta$$
$$+ (\cos\psi - \cos\varphi\sin\psi\tan\theta)^2 \quad (28)$$

In this case, we can estimate the zonal irregularity drift as

$$V_D = V_{D0} \pm V_{D1} \quad (29)$$

where

$$V_{D0} = V_{py} + \frac{(V_{px}\sin\psi - V_{pz}\cos\psi)\sin\varphi\tan\theta}{\cos\psi - \cos\varphi\sin\psi\tan\theta} \quad (30)$$

and

$$V_{D1} = \sqrt{1 + \frac{\sin^2\varphi\tan^2\theta}{(\cos\psi - \cos\varphi\sin\psi\tan\theta)^2}}\, V_{eff} \quad (31)$$

As with the finite axial ratio model, in (30) V_{D0} is generally on the order of 40 m/s for GPS satellite orbits in the equatorial zone where the irregularities are highly elongated. Thus, when the irregularities are drifting eastward at speeds exceeding 40 m/s

(which is typical) the positive root should be chosen in (29).

For sufficiently high elevation satellites $V_{D0} \approx V_{py}$ and the second term inside the radical in (31) can be neglected, so that $V_{D1} \approx V_{eff}$. In this case the effective velocity in (27) reduces to $V_{eff} \approx |V_D - V_{py}|$ and the angles φ and ψ no longer play a role. Under these conditions, the zonal irregularity drift can be estimated simply as $V_D = V_{py} \pm V_{eff}$.

Another simplification worth mentioning is the case of a geostationary satellite for which the penetration point motion may be neglected. In this case, equations (29-30) imply that $V_{D0}=0$. We note, however, that while the GNSS geostationary satellites used for SBAS are in geostationary orbits they may not be used with this technique since the transmitted phase is intentionally modulated and σ_φ cannot be measured.

We can summarize the finite axial ratio model with a single expression (which also may be considered a principal result of this paper):

$$V_D \approx V_{py} + \frac{(V_{px}\sin\psi - V_{pz}\cos\psi)\sin\varphi\tan\theta}{\cos\psi - \cos\varphi\sin\psi\tan\theta}$$
$$\pm \sqrt{1 + \frac{\sin^2\varphi\tan^2\theta}{(\cos\psi - \cos\varphi\sin\psi\tan\theta)^2}} \quad (32)$$
$$\cdot \frac{\rho_F}{\tau_c} Q_\sigma(p)\left[\frac{\sigma_\varphi}{S_4}\right]^{\frac{2}{p-1}}$$

The first two terms in (32) account for satellite motion and depend on the magnetic field orientation at the IPP. The third term accounts for the scintillation and depends on the scattering layer height and phase spectral index of the irregularities.

The zonal irregularity drifts reported in the next section were computed in two ways, first assuming an axial ratio of the irregularities along and across magnetic field lines is 50:1, and the second assuming infinitely long irregularities and the simple model given in (32). The difference between the finite and infinite axial ratio models was less than 4 m/s (8 m/s) for satellites with el>45° (el>30°). Thus, we find that is largely unnecessary to use the more complex finite

axial ratio model for the highly elongated irregularities characteristic of the disturbed equatorial ionosphere.

Summary of the Algorithm

In summary, one can estimate the zonal irregularity drift using a stand-alone GNSS scintillation monitor at low latitude station by following these steps.

1. Specify the height of the scattering layer (350-450 km is typical) and compute the Fresnel scale for each satellite link using (4).
2. Measure S_4 and either T or σ_φ along each satellite link and compute the corresponding effective scan velocities using either the finite axial ratio model, (10) and (15), or the infinite axial ratio model, (23) and (24), respectively.
3. Compute the velocity of the ray-path at the IPPs by using standard GPS ephemeris. Compute the magnetic field angles at the IPP locations and rotate the ray-path velocities into magnetic coordinates to find V_{px}, V_{py}, and V_{pz}. From these, compute V_{sx0} and V_{sy0} using (18).
4. From the magnetic field angles and propagation direction, compute the propagation geometry parameters A, B, and C, using equation (40) and the combined propagation and geometry factor $\wp(p)$ using equation (45) in the Appendix.
5. Solve the quadratic equation for the zonal irregularity drift using equation (19). For irregularities drifting eastward faster than 40 m/s, the positive sign for the radical should be used.

Alternatively, one may use the single equation form of the infinite axial ratio model given in (32).

3. DATA ANALYSIS

For this study, we used GPS observations and VHF spaced-receiver measurements from the SCINDA network owned and maintained by Air Force Research Laboratory (AFRL). We consider data from three SCINDA stations in the equatorial zone,

Bangkok (BKK), Cape Verde (CVD), and Kwajalein Atoll (KWA). The geographic coordinates and magnetic dip angles of these stations are listed in Table 1.

Table 1. Geographic coordinates and magnetic dip angles for the stations considered in this study.

Station	Lat.	Lon.	Dip Angle
Bangkok (BKK)	14.1°N	100.6°E	14.0°N
Cape Verde (CVD)	16.73°N	22.9°W	18.5°N
Kwajalein (KWA)	9.4°N	167.5°E	8.5°N

Each of these stations is equipped with a NovAtel GSV4004B scintillation monitor that reports S_4 and σ_φ measurements every 60 seconds. The S_4 values have been corrected to remove the contribution due to thermal noise, as described in Van Dierenonck et al. [1993]. The σ_φ values are computed (in receiver firmware) from the detrended carrier phase measurements using a 6th order Butterworth high-pass filter with 3dB cutoff at $\tau_c = 10$ seconds. The data for 4 minutes following each receiver-detected cycle slip is discarded to avoid spurious transients produced by the detrending filter. To avoid contamination by multipath from terrestrial objects, data from satellites below 30° in elevation are discarded. To minimize the influence of receiver noise, data for which $S_4 < 0.35$ or $\sigma_\varphi < 0.05$ are discarded. To ensure the weak scatter theory is applicable, data for which $S_4 > 0.8$ or $\sigma_\varphi > 1.0$ are discarded.

The spaced VHF receiver measurements of zonal irregularity drift were obtained by cross-correlation of the intensity fluctuations measured from 250 MHz geostationary links by receivers separated in the magnetic east-west direction, as described by Spatz et al. [1988]. The ionospheric penetration points of the VHF links at stations BKK, CVD, and KWA are located at 98.8°E, 22.9°W, and 168.3°E, respectively.

We assume the irregularities have spectral index p=3. As discussed before, the assumed altitude of the scattering layer is expected to affect the bias of the estimated zonal drift. We found that choosing 400 km

for Bangkok and Cape Verde produced GPS drift estimates with little bias. The higher altitude of 450 km was needed at Kwajalein to achieve a low bias.

The results for Bangkok, Cape Verde, and Kwajalein are shown in Figures 1, 2, and 3, respectively. These figures each compare the zonal irregularity drift for three evenings measured with spaced VHF antennas and a stand-alone NovAtel GSV4004B scintillation monitor.

The agreement between the GPS and VHF drift measurements is generally good, although occasional outliers do occur. Outliers in which the GPS overestimates the drift may be caused by increased phase noise or small undetected cycle slips. We note that the VHF drift estimates are made by sampling the sky in a single direction (i.e. toward the geostationary satellite whose signal is being monitored). The GPS drift estimates, on the other hand, are made by sampling the sky in all directions (toward the GPS satellites). Some of the differences between the GPS and VHF drift measurements may be attributed to real longitudinal gradients in the zonal irregularity drift (which the GPS system can capture but the VHF system cannot).

Next, we validated the GPS zonal drift estimates by comparing them with the VHF spaced antenna zonal drift data during the period 1-30 Nov 2013. Not all of these evenings were accompanied by scintillation. Since the epochs of the VHF and GPS drift estimates are not temporally aligned, we used the following approach to compare them. First, we calculated the median drift from the VHF samples in 5 minute bins. Using the median VHF drift as a reference (since no independent and more reliable measure of the drift was available for validation), we interpolated it to epochs of the VHF and GPS measurements. We then computed the "error" as the distance (in m/s) between the VHF and GPS drift estimates and this reference. We note that this "error" has zero bias for the VHF measurements, by construction, and while it may not represent an actual measurement error for the VHF, it does characterize the spread of the measurements about their mean.

The statistical distribution of these errors is shown in the form of histograms for Bangkok, Cape Verde,

and Kwajalein in Figures 4, 5, and 6, respectively. The histograms show the occurrence frequency of the absolute errors (signed, but not normalized by the reference) and relative errors for the GPS and VHF estimated drifts shown in solid red and cross-hatched blue bars, respectively. The filled triangle near the abscissa scale shows the mean value of the GPS drift estimates, while the unfilled triangles show +/- 1 standard deviation.
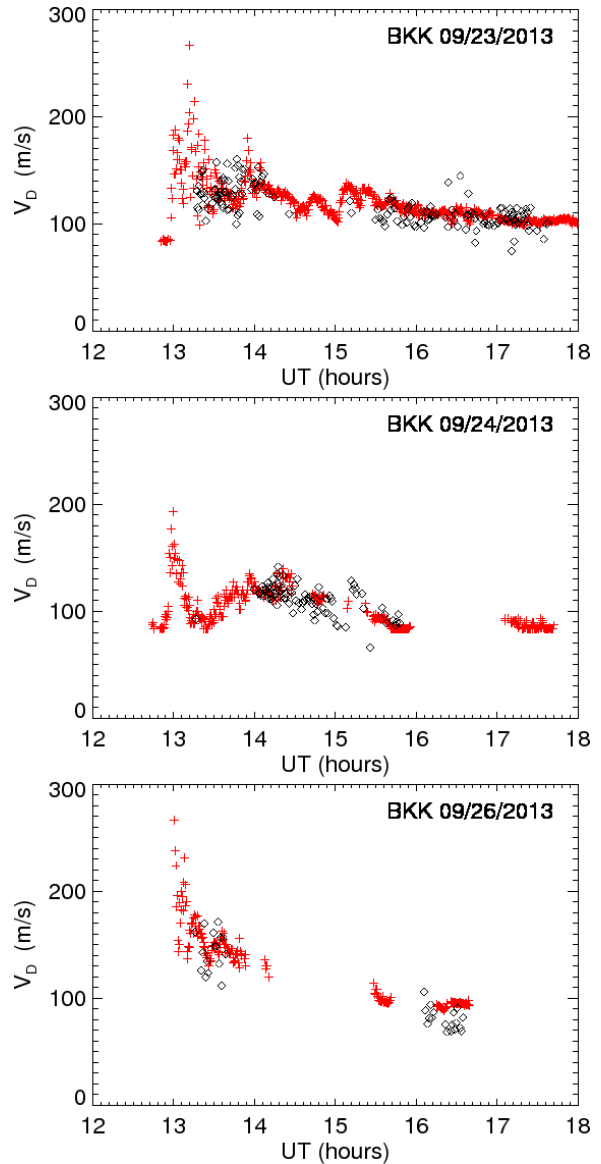

Figure 1. Zonal irregularity drift for three evenings at Bangkok measured with spaced VHF antennas (red crosses) and a stand-alone GPS receiver (black diamonds).
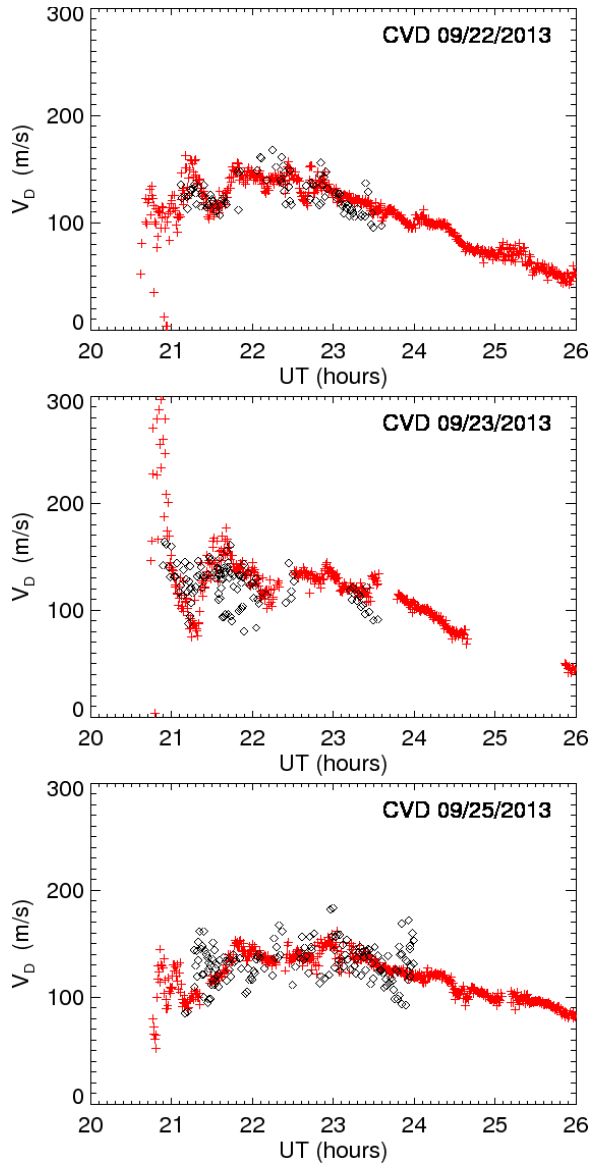
Figure 2. Zonal irregularity drift for three evenings at Cape Verde measured with spaced VHF antennas (red crosses) and a stand-alone GPS receiver (black diamonds).

To avoid artificially inflating the errors due to possible longitudinal gradients in the zonal drift, when generating these histograms we retained only GPS samples for which the IPP lies within +/- one degree in longitude from the IPP of the VHF satellite IPP. We also discarded the first 20 minutes of VHF drift estimates from the validation, as these are often spurious (presumably because the bubbles have a significant vertical velocity component at this time, which is not accounted for when estimating the drift).
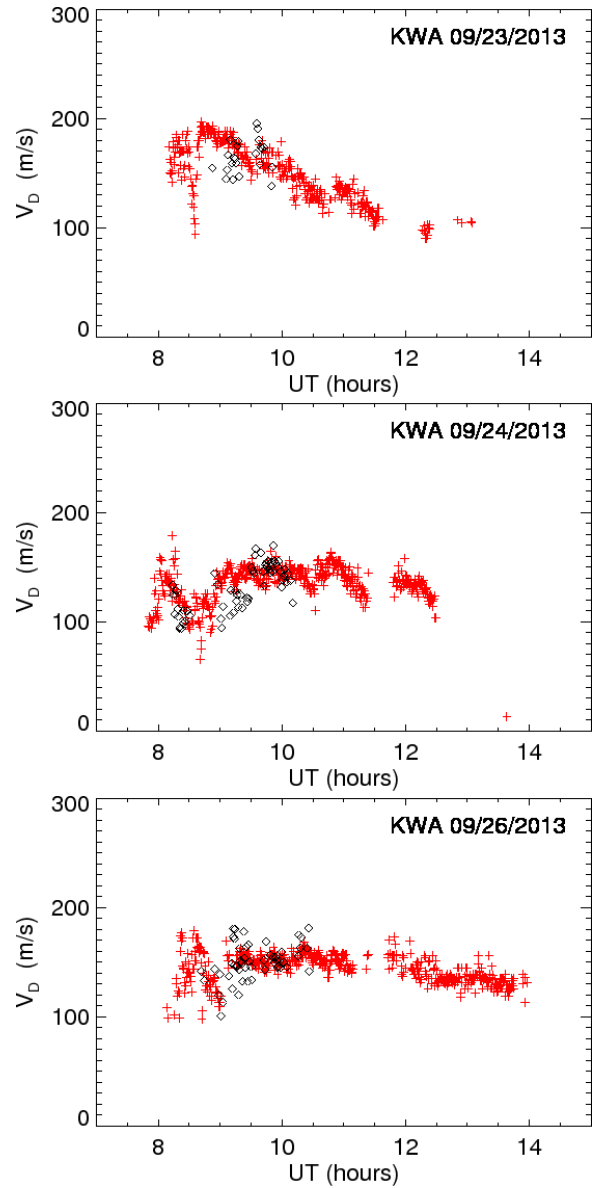

Figure 3. Zonal irregularity drift for three evenings at Kwajalein measured with spaced VHF antennas (red crosses) and a stand-alone GPS receiver (black diamonds).
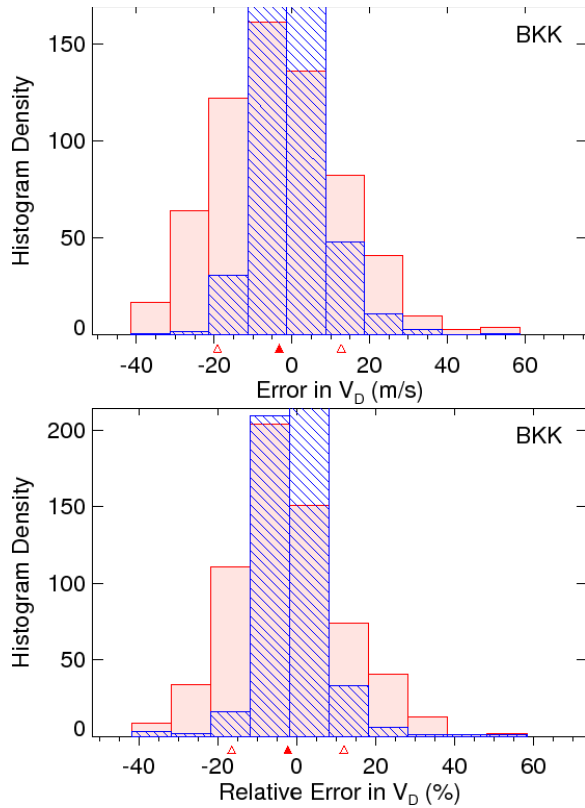
Figure 4. Histograms of the errors (top) and relative errors (bottom) in the zonal irregularity drift for 1-30 Nov 2013 at Bangkok estimated with VHF (cross-hatched blue and GPS (solid red).
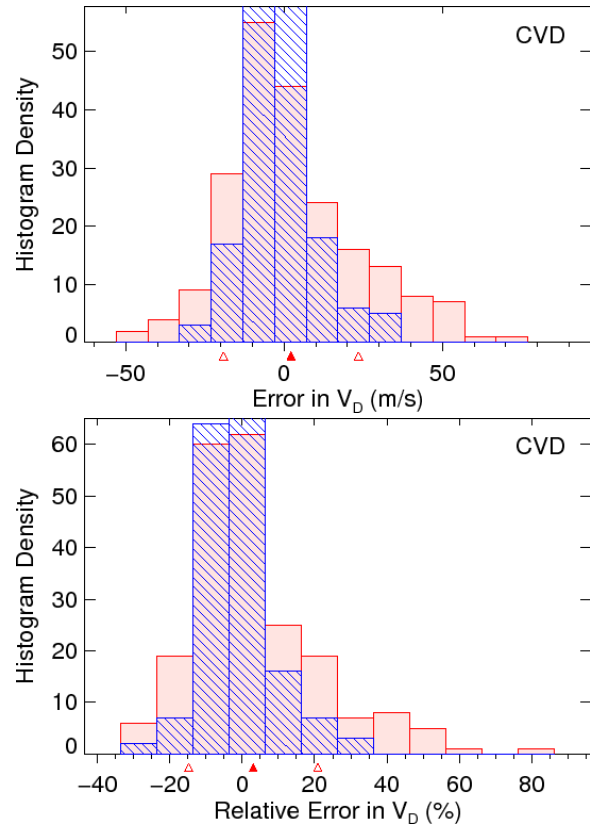

Figure 5. Histograms of the errors (top) and relative errors (bottom) in the zonal irregularity drift for 1-30 Nov 2013 at Cape Verde estimated with VHF (cross-hatched blue and GPS (solid red).

We can summarize these error histograms as follows. At all three stations the mean errors in the GPS drift estimates were very small (<3 m/s). These small biases could be misleading, in the sense that we intentionally adjusted the assumed value for scattering later height in order to achieve a small bias. At station BKK the GPS drift errors had standard deviation 15.9 m/s and relative standard deviation 14.2%. These can be compared with the VHF drift estimates which had standard deviation 10.1 m/s and relative standard deviation 6.9%. At station CVD the GPS drift errors had standard deviation 21.3 m/s and relative standard deviation 17.9%. These can be compared with the VHF drift estimates which had standard deviation 9.7 m/s and relative standard deviation 8.3%. Finally, at station KWA the GPS drift errors had standard deviation 19.6 m/s and relative standard deviation 13.0%. These can be compared with the VHF drift estimates

which had standard deviation 13.7 m/s and relative standard deviation 12.5%.

Roughly speaking, the GPS drift estimates have approximately 60-70% larger scatter about their mean as compared to the VHF estimates. Nevertheless, we consider this result quite encouraging given the numerous assumptions required to compute them (principally the spectral index and scattering layer height). We believe that the statistical tail comprised of overestimated drift measurements from the GPS (e.g. Figures 4 and 5) may be due, at least in part, to increased receiver phase noise or undetected cycle slips. To establish whether or not this is the case, we will need to carefully scrutinize the high rate phase data in a future study.
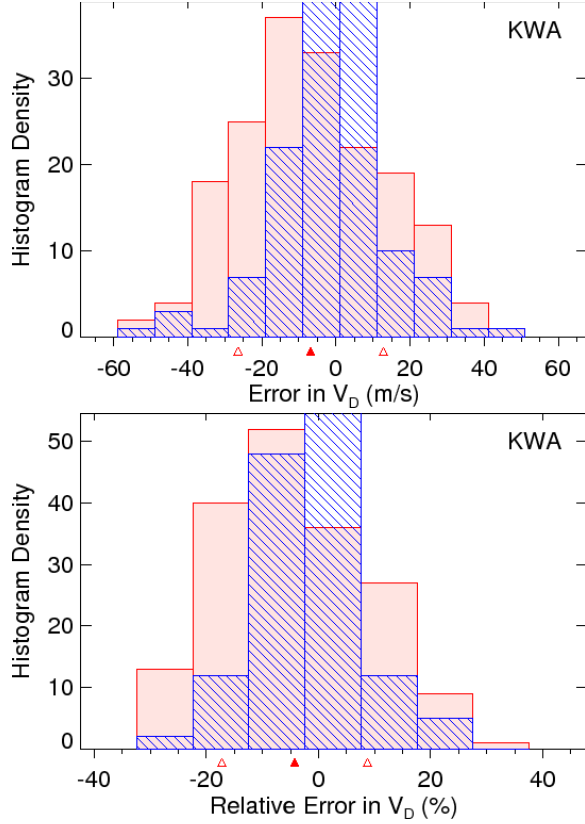
Figure 6. Histograms of the errors (top) and relative errors (bottom) in the zonal irregularity drift for 1-30 Nov 2013 at Kwajalein estimated with VHF (cross-hatched blue and GPS (solid red).

4. ERROR ANALYSIS AND DISCUSSION

Application of the current technique for estimating the zonal irregularity drift requires several conditions be met, which we review here. First, both S_4 and σ_φ must be small (i.e. the weak scatter theory must apply). Moreover, they must include negligible contributions from multipath and receiver noise compared to that due to scintillation. We can ensure the former condition by rejecting samples from low elevation satellites and we can ensure the latter by rejecting measurements of S_4 and σ_φ which are too close to the noise floor. We must provide a guess at the scattering height, which is generally unknown. The result will bias the estimated drift measurements, but at least the dependence on height is of the square root type. We must also assume the spectral index of the irregularities, which is also unknown, although a

value of $p=3$ appears to provide satisfactory results. To use the integral approximation (11) the detrend filter cutoff τ_c must be shorter than the outer scale time constant. This condition effectively places an upper bound on the zonal drift speeds that can be measured (although this limitation can be circumvented by retaining the outer scale in the integration). The infinite axial ratio model in (32) assumes highly elongated rod-like irregularities characteristic of the equatorial ionosphere, which may not be appropriate for auroral or polar cap structures. Both formulations assume purely zonal drift, which is approximately valid in the equatorial zone following the initial development stage of the turbulence, but not at high-latitudes.

At this point we add some further conditions, not to enable measurement of the drift but to help interpret the behavior of the technique. First, we observe that when $p=3$ (which is typical of the low-latitude ionosphere) we have $Q_T(p) = Q_\sigma(p) = 2\pi^{3/2} \approx 11.1$. If we further assume a fixed $\tau_c=10$ second detrend filter cutoff (this is the default value used by the GSV4004B scintillation monitor), then equations (23) and (24) become simply:

$$V_{eff} = 11.1 \rho_F \frac{T^{1/2}}{S_4} \qquad (33)$$

and

$$V_{eff} = 1.11 \rho_F \frac{\sigma_\varphi}{S_4} \qquad (34)$$

The latter form is the easiest form to interpret, and says that the effective scan velocity is very nearly equal (except for the factor of 1.11) to the Fresnel scale times the ratio of σ_φ to S_4.

For the moment, assume that we have specified the phase spectral index correctly and wish to know how errors in the estimated drift depend on our selection of the scattering layer height. From (4) and (34), the relative error in the effective scan velocity estimation due to an incorrectly chosen scattering layer height is

$$\frac{V_{eff} - V_{eff}^*}{V_{eff}^*} = \sqrt{\frac{z}{z^*}} - 1 \qquad (35)$$

where z^* and V_{eff}^* represent the true (unknown) altitude of the scattering layer and effective scan velocity, respectively. For the case of vertical propagation with an infinite axial ratio, $V_D = V_{py} +/- V_{eff}$, and provided $|V_{eff}|>>|V_{py}|$ (which is typical for GPS satellite scans in the low-latitude ionosphere) then the condition (35) on V_{eff} applies to V_D as well, namely

$$\frac{V_D - V_D^*}{V_D^*} = \sqrt{\frac{z}{z^*}} - 1 \qquad (36)$$

The above implies that if the scattering layer height is underestimated (overestimated), the inferred irregularity drift will be underestimated (overestimated). However, the square-root dependence on the scattering layer height makes the drift is relatively insensitive to this parameter. We should point out, however, that in this simplistic analysis we have neglected the height dependence of the IPP location and magnetic field orientation, which we assume to be second order effects.

We note that Cerruti et al. (2006) used a similar approach to infer the scattering later height given the zonal irregularity drift and measurements of the diffraction pattern on the ground. These authors noted an extreme sensitivity of their estimated scattering height to the zonal irregularity drift (a 6 m/s error in measuring the drift resulted in a 100 km error in the scattering height). Our methodology is different from theirs (and the coupling between the drift and layer height in our model is less severe), but the philosophy is also different. Since the diffraction pattern sampled at the receiver is more sensitive to the irregularity velocity than the scattering height, it is more accurate to guess the latter and estimate the former. The present method capitalizes on this to provide reasonably accurate measurements of zonal drift even when the scattering height is imprecisely known.

Now assume that we have specified the scattering layer height correctly and wish to know how errors in the estimated drift depend on our selection of the phase spectral index. From (24) we can write

$$\frac{V_{eff} - V_{eff}^*}{V_{eff}^*} = \frac{Q_\sigma(p)}{Q_\sigma(p^*)} \left(\frac{\sigma_\varphi}{S_4} \right)^{e(p,p^*)} - 1 \qquad (37)$$

where the exponent is given by

$$e(p, p^*) = \frac{2(p^* - p)}{(p^* - 1)(p - 1)} \qquad (38)$$

and p^* and V_{eff}^* represent the true (unknown) phase spectral index and effective scan velocity, respectively. As before, if we assume vertical propagation, infinite axial ratio, and $|V_{eff}|>>|V_{py}|$ then the condition (37)-(38) on V_{eff} applies to V_D as well. Even with these restrictions, the relative error bears a more complex dependence on spectral index than scattering layer height. However, we can get an idea of how the error behaves as follows. Suppose, in addition, that the true spectral index is $p^*=3$ and the measured ratio σ_φ / S_4 ranges from 0.25 to 2.0. Then the predicted errors in measuring the zonal irregularity drift would look like those shown in Figure 7. Each curve shown in the figure corresponds to a different value of the measured ratio σ_φ / S_4. Note how the errors are asymmetrical with respect to the true spectral index $p^*=3$.

The error histograms shown in Figures 4-6 are fairly symmetrical (i.e. the statistical skewness is low) and were produced assuming $p=3$. Most of the σ_φ / S_4 values we measured were smaller than one. When we experimented with p values smaller than 3 the error histograms (not shown) were skewed toward negative drift errors (i.e. there were more samples underestimating the correct drift than overestimating the correct drift). Conversely, when we experimented with p values greater than 3 the error histograms (not shown) were skewed toward positive errors. This behavior is consistent with the predicted errors shown in Figure 7 when σ_φ / S_4 is less than one. Most of the instances where the drift was significantly over-predicted were associated with σ_φ / S_4 measurements exceeding one. Lastly, the magnitudes of the drift errors we observed are consistent with the predicted errors shown in Figure 7. We can conjecture from this analysis that a significant contribution to the drift errors likely originates from the natural variability in

phase spectral index that is observed at low latitudes [Carrano et al., 2014].
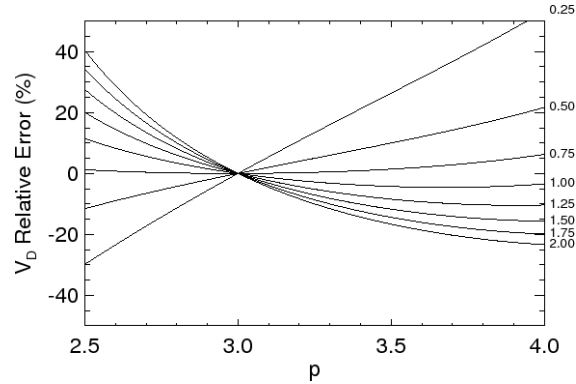

Figure 7. Predicted dependence of the relative error in estimating the zonal irregularity drift due to incorrect specification of the phase spectral index. The curves are labeled with the measured value of the ratio σ_φ / S_4.

The specialization of Rino's formulas to the case of infinitely elongated rod-like field-aligned irregularities allows for easy numerical evaluation of the technique and also facilitates the interpretation of its behavior. We emphasize that the infinite axial ratio model is suitable for the equatorial zone only. At auroral latitudes where irregularities may form sheet-like structures one should use the general forms (10) or (15) instead.

Finally, we note that for nearly vertical propagation with p=3 and τ_c=10 sec the infinite axial ratio model (32) can be manipulated to give

$$\frac{\sigma_\varphi}{S_4} \approx \frac{V_D - V_{py}}{1.11\rho_F} \qquad (39)$$

This simple result is a useful rule of thumb for the behavior of S_4 and σ_φ measurements provided by a GNSS scintillation monitor. As is well known, S_4 depends on the distance to the irregularities through the Fresnel scale. It does not depend on the irregularity drift or the satellite scan velocity. On the other hand, σ_φ is directly proportional to the relative difference between the zonal irregularity drift and magnetic eastward component of the IPP motion. Changing the perturbation strength affects both S_4 and σ_φ but not their ratio (provided the weak scatter

assumption is valid). This being said, studies in the literature which measure S_4 and σ_φ as if they were independent parameters are misleading; in fact these parameters are closely related through the relative drift and Fresnel scale.

5. CONCLUSIONS

We present a new approach that leverages the weak scatter scintillation theory [Rino et al., 1979] to infer the zonal irregularity drift from measurements of S_4 σ_φ provided by a stand-alone GNSS scintillation monitor. We evaluated the accuracy of this approach by comparing GPS estimates of zonal irregularity drift with VHF spaced-receiver measurements collected at three low-latitude stations of the AFRL-SCINDA network. By careful selection of the scattering layer height and spectral index, we were able to obtain GPS estimates of the zonal irregularity drift that were unbiased and with a spread about the mean of 16-21 m/s (13-18% relative error), which is roughly 60-70% larger that observed with the VHF spaced-receiver measurements. A simple error analysis of the technique suggests that errors in the assumed scattering layer height result in an overall drift bias, whereas the spread of the drift estimates is likely due to the natural variability of the phase spectral index in at low latitudes (which we neglect by assuming a fixed value).

We also noted that a simplified version of the model, which assumes infinitely elongated rod-like irregularities, provides drift measurements within 4 m/s (8 m/s) for satellites above 45° (30°) elevation compared with the more general finite axial ratio model. These results suggest the infinite axial ratio model is a useful description of irregularities in the equatorial ionosphere. This simplified model not only facilitates the drift calculations, but it also aids in the interpretation of the technique and the inter-connections between zonal irregularity drift, Fresnel scale, and measurements of σ_φ and S_4 provided by a GNSS scintillation monitor operating in the equatorial ionosphere.

We emphasize that the present method provides a model-inferred drift and is not intended to supplant direct measurements of the zonal irregularity drift made by the spaced-receiver technique. Furthermore,

because of the frequency dependence of scintillation, VHF sensors are inherently more sensitive to scintillation than GPS sensors. As a result, the VHF systems can monitor the drift of much weaker plasma irregularities which commonly persist late into the evening. Despite these shortcomings, the current technique should prove useful for the vast majority of GNSS scintillation monitors which are situated too distant from other neighboring scintillation monitors to apply the spaced-receiver technique. The SCINDA and the LISN networks respectively have 25-30 and 35-50 simultaneously operating GNSS scintillation monitors which are suitable for measuring the zonal irregularity drift with the current technique.

In this study we selected the scattering height to provide unbiased drift estimates using the VHF spaced-receiver drift measurements as "calibration." Under normal circumstances, the scattering height would not be known and nor would external calibration data be available to guide in its selection. However, the error in the drift estimates obtained with this technique has a square root dependence on the scattering height, so that reasonable accuracy in the drift can be achieved when the scattering height is imprecisely known. Still, this technique could potentially benefit from an external source of information regarding the scattering layer height. A nearby ionosonde could provide measurements of HmF2 just prior to development of spread F which may be presumed to be closely related to the height at which L-band signals are scattered. Better still would be direct measurements of scattering height from a coherent backscatter radar.

In future work, we plan to incorporate additional data sources to accurately specify the two model parameters which were simply assumed here, namely the scattering height and the phase spectral index. If we apply this GPS technique at Kwajalein during evenings when the ALTAIR radar is operating and observing coherent echoes, the radar could provide the scattering layer height. An analysis of high rate GPS phase observations at Kwajalein could be used to specify the spectral index.

6. APPENDIX

The coefficients A, B, and C in Rino's model depend on the directions of propagation and the magnetic field. They are obtained by relating the propagation direction and the irregularity axes [Rino, 1979]:

$$
\begin{aligned}
A &= C_{11} + C_{33}\tan^2\theta\cos^2\varphi - 2C_{13}\tan\theta\cos\varphi \\
B &= 2\,[C_{12} + C_{33}\tan^2\theta\sin\varphi\cos\varphi \\
&\quad - \tan\theta\,(C_{13}\sin\varphi + C_{23}\cos\varphi)] \\
C &= C_{22} + C_{33}\tan^2\theta\sin^2\varphi - 2C_{23}\tan\theta\sin\varphi
\end{aligned}
\tag{40}
$$

where

$$
\begin{aligned}
C_{11} &= a^2\cos^2\psi + \sin^2\psi\,(b^2\sin^2\delta + \cos^2\delta) \\
C_{22} &= b^2\cos^2\delta + \sin^2\delta \\
C_{33} &= a^2\sin^2\psi + \cos^2\psi\,(b^2\sin^2\delta + \cos^2\delta) \\
C_{12} &= (b^2-1)\sin\psi\sin\delta\cos\delta \\
C_{13} &= (a^2 - b^2\sin^2\delta - \cos^2\delta)\sin\psi\cos\psi \\
C_{23} &= -(b^2-1)\cos\psi\sin\delta\cos\delta
\end{aligned}
\tag{42}
$$

In the above, ψ is the magnetic inclination angle at the IPP and δ is the angle at which irregularities are inclined from the xz plane (typically taken to be zero at low latitudes). We use the IGRF model to compute the magnetic inclination and declination at the ionospheric penetration points.

The geometry enhancement factor G is defined in Rino [1979] equation (10), but note that the cos theta term does not belong under the radical as was printed in that paper. The correct equation is

$$
G = \frac{ab}{\cos\theta\sqrt{AC - B^2/4}}
\tag{44}
$$

The combined geometry and propagation factor is given by

$$
\begin{aligned}
\wp(p) &= \frac{ab}{\sqrt{A''C''^{\,p/2}}} \\
&\quad {}_1F_2\left[(1-p)/2,\,1/2;\,1;\,(A''-C'')/A''\right]
\end{aligned}
\tag{45}
$$

where ${}_1F_2\left[\cdot\right]$ is the Gauss hypergeometric function. The geometrical coefficients appearing in (45) are defined by the equations below:

$$A' = (A\cos^2\varphi + B\cos\varphi\sin\varphi + C\sin^2\varphi)\cos^2\theta$$
$$B' = (B\cos 2\varphi + (C-A)\sin 2\varphi)\cos\theta \qquad (46)$$
$$C' = A\sin^2\varphi - B\cos\varphi\sin\varphi + C\cos^2\varphi$$

$$D' = \sqrt{(C'-A')^2 + B'^2} \qquad (47)$$

$$A'' = \left[A' + C' + D'\right]/2$$
$$C'' = \left[A' + C' - D'\right]/2 \qquad (48)$$

AKNOWLEDGEMENTS

REFERENCES

Carrano, C. S., C. E. Valladares, and K. M. Groves (2012a), Latitudinal and local time variation of ionospheric turbulence parameters during the Conjugate Point Equatorial Experiment in Brazil, Int. Journal of Geophysics, vol. 2012, Article ID 103963, 16 pages, doi:10.1155/2012/103963.

Carrano, C. S., K. M. Groves, W. J. McNeil, and P. H. Doherty (2012b), Scintillation characteristics across the GPS frequency band, Proceedings of the 2012 Institute of Navigation ION GNSS meeting, Nashville, TN, September 17-21, 2012.

Carrano, C. S., K. M. Groves, W. J. McNeil, and P. H. Doherty (2013), Direct measurement of the residual in the ionosphere-free linear combination during scintillation, Proceedings of the 2013 Institute of Navigation ION NTM meeting, San Diego, CA, January 28-30, 2013.

Carrano, C. S., K. M. Groves, S. H. Delay, and P. H. Doherty (2014), An Inverse Diffraction Technique for Scaling Measurements of Ionospheric Scintillations on the GPS L1, L2, and L5 Carriers to Other Frequencies, Proceedings of the 2014 Institute of Navigation ION ITM meeting, San Diego, California, January 27-29, 2014.

Cerruti, A. P., B. M. Ledvina, and P. M. Kintner (2006), Scattering height estimation using scintillating Wide Area Augmentation System/Satellite Based Augmentation System and GPS satellite signals, Radio Sci., 41, RS6S26, doi:10.1029/2005RS003405.

de Paula, E.R., et al. (2002), Ionospheric irregularity zonal velocities over Cachoeira Paulista, J. Atmos. and Solar-Terr. Phys. 64, 1511–1516.

Ji, S., W. Chen, X. Ding, and C. Zhao (2011), Equatorial ionospheric zonal drift by monitoring local GPS reference networks, J. Geophys. Res., 116, A08310, doi:10.1029/2010JA015993.

Ledvina, B. M., P. M. Kintner, and E. R. de Paula (2004), Understanding spaced-receiver zonal velocity estimation, J. Geophys. Res., 109, A10306, doi:10.1029/2004JA010489.

Liang, X.U., X.U. Ji-Sheng, Z. Jie, Z. Yu-Hua, L. Si-Min (2009), GPS measurements of ionospheric irregularity drifts and their initial results, Chinese journal of geophysics vol.52, no.1, pp: 1-12.

Rino, C. (1979), A power law phase screen model for ionospheric scintillation, 1 Weak scatter, Radio Sci., 14, 1135-1145.

Secan, J. A., R. M. Bussey, E. J. Fremouw, and S. Basu (1995), Improved model of equatorial scintillation, Radio Sci.,30, 3, pp. 607–617, 1995.

Spatz, D. E., S. J. Franke, and K. C. Yeh (1988), Analysis and interpretation of spaced receiver scintillation data recorded at an equatorial station, Radio Sci., 23, 3, 347-361, 1998.

Vacchione, J. D., Franke, S. J., and K. C. Yeh (1987), A new technique for estimating zonal irregularity drifts and variability in the equatorial F region using spaced receiver scintillation data, Radio Sci., 22, 5, 745-756, 1987.

Van Dierendonck, A. J., J. Klobuchar, and Q. Hua (1993), Ionospheric scintillation monitoring using commercial single frequency C/A code receivers, paper presented at ION GPS-93, Inst. of Navig., Arlington, Va., Sept.